Int. J. Electrochem. Sci., 13 **(2018)** 7706 – 7717, doi: 10.20964/2018.08.22

International Journal of
ELECTROCHEMICAL
SCIENCE
www.electrochemsci.org

Effect of Friction on Preparation of NdFeB Nickel Coating by Jet Electrodeposition

Xin Wang[1], *Lida Shen*[1,*], *Mingbo Qiu, Kai Wang, Zongjun Tian*

College of Mechanical and Electrical Engineering, Nanjing University of Aeronautics and Astronautics, No. 29 Yudao Street, Nanjing, Jiangsu 210016, PR China.
[1] These authors contributed equally to this work.
[*]E-mail: ldshen@nuaa.edu.cn

Received: 18 April 2018 / *Accepted:* 31 May 2018 / *Published:* 5 July 2018

Sintered neodymium (NdFeB) magnets are highly vulnerable to corrosion. To address this problem, flexible friction-assisted jet electrodeposition is applied. This technique can effectively and quickly prepare protective Ni coating on NdFeB magnets. Three kinds of jet electrodeposition are compared: non-friction, fixed friction-assisted and movable friction-assisted jet electrodeposition. The surface morphology of Ni coating is examined by scanning electron microscopy. X-ray diffraction is employed to evaluate the effect of friction on tissue structure. Corrosion of the nickel coating is characterized using an electrochemical workstation. Results indicate that flexible, movable friction improves the morphology of the jet-electrodeposited surface, and exhibits a (111) preferred orientation. In addition, compared with fixed friction, flexible, movable friction provides coatings with higher adhesion strength. Jet electrodeposition with flexible, movable friction also provides excellent corrosion resistance for the sintered NdFeB magnets, and corrosion current decreases from 104.5μA/cm^2 to 28.75 μA/cm^2.

Keywords: jet electrodeposition, flexible friction, anticorrosion, NdFeB

1. INTRODUCTION

NdFeB is a type of material with extremely high magnetic energy product and coercivity. Owing to its high energy density, NdFeB is widely used in modern industries and electronics technology[1-4]. However, sintered NdFeB exhibits poor corrosion resistance. The active phase, such as the Nd-rich phase and B-rich phase in NdFeB permanent magnets, facilitates corrosion in corrosive media and weakens the magnetic properties of the material, limiting its application[5, 6]. To enhance the corrosion resistance of sintered NdFeB materials, experiments have been conducted, such as the addition of Co, Dy, Nb, and other alloying elements; however, the NdFeB metallographic phase is

typically changed[7, 8]. Cathodic arc physical vapor deposition titanium nitride coating is used in the industry to improve the corrosion resistance of NdFeB[9]. Electroless deposition of the Ni-P multilayer film on the NdFeB substrate can increase corrosion resistance[10, 11]; however, these processes are highly complex.

Electroplating is one of the most commonly used approaches and has been widely applied as a conventional surface treatment with several advantages, such as simplicity of the process flow, satisfactory corrosion performance, and low cost. However, traditional electrodeposition methods include disadvantages, such as low current density, low deposition rate, and surface defects[12-17]. To improve the properties of the deposited layer, experiments have been conducted, includes Ultrasound-assisted[18-20], nanocomposite coatings technique[21-23] and so on. Compared with traditional electrodeposition, jet electrodeposition with its excellent mass transfer characteristics and ability to reduce the thickness of the diffusion layer increases the limiting current density and substantially increases the efficiency of electrodeposition[15-18, 22-24]. However, at a higher current density, the surface of the coating produced by jet electrodeposition still shows defects. These defects, such as protrusions or sipes, affect the corrosion resistance of the coating. A flexible, movable friction-assisted technology is introduced in this study to obtain high-quality coatings and thus improve the quality of electrodeposition. An on-line assisted friction device is designed using natural bristle[25, 26] as a flexible friction medium. High-efficiency and high-performance jet electrodeposition is used on the NdFeB substrate to produce Ni coating in order to improve its anticorrosion performance and material life.

2. EXPERIMENTAL SYSTEM

2.1 Experimental devices

The experimental device is shown in Fig. 1. The controllable jet electrodeposition system consists of three parts: the control system, the bath circulation system and the XZ-axis platform. The workpiece (NdFeB) is mounted on the XZ-axis platform with the use of special fixture. The movement of the fixture is controlled by a program to regulate the scanning range of the workpiece, scanning speed, and deposition time of jet electrodeposition. The electroplating solution is pumped from the electroplating bath into the anode chamber and then sprayed on the workpiece surface from the jet nozzle. A nickel rod is inserted into the anode chamber and then connected to the anode of the power supply. The anode cavity is simultaneously filled with nickel beads to prepare for anode consumption during electrodeposition, thereby reducing nickel ion loss in the plating bath. Throughout the electrodeposition process, the nozzle remains stationary, and the workpiece moves in a reciprocating manner in the X direction with a stepper motor to complete the deposition on one plane.

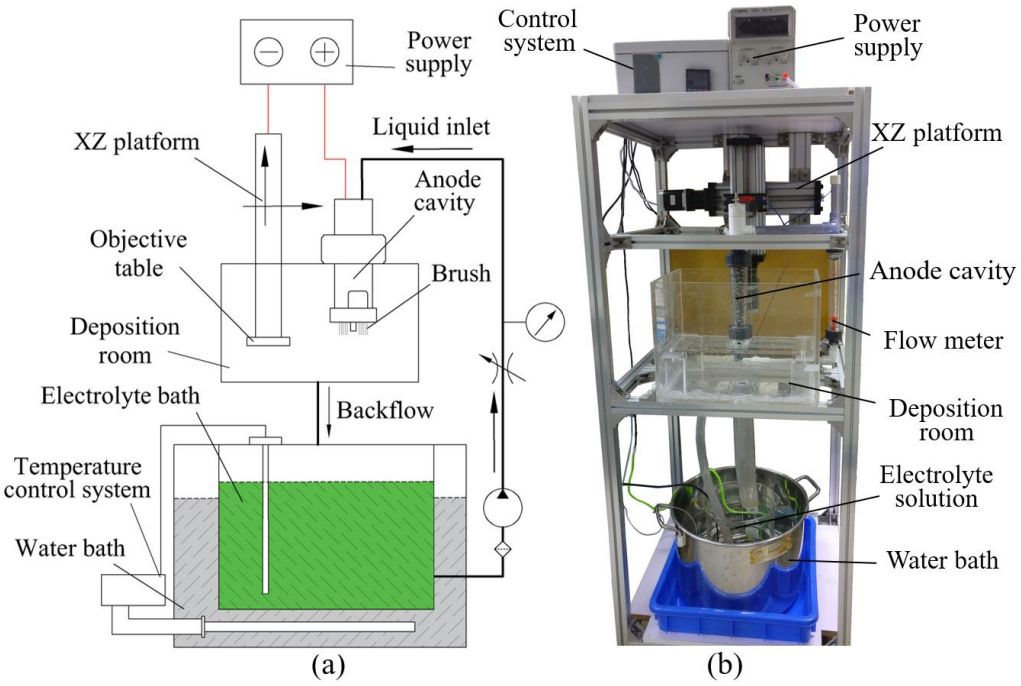

Figure 1. Experiment device (a) Schematic diagram, (b) Scene photograph.

2.2 Friction devices

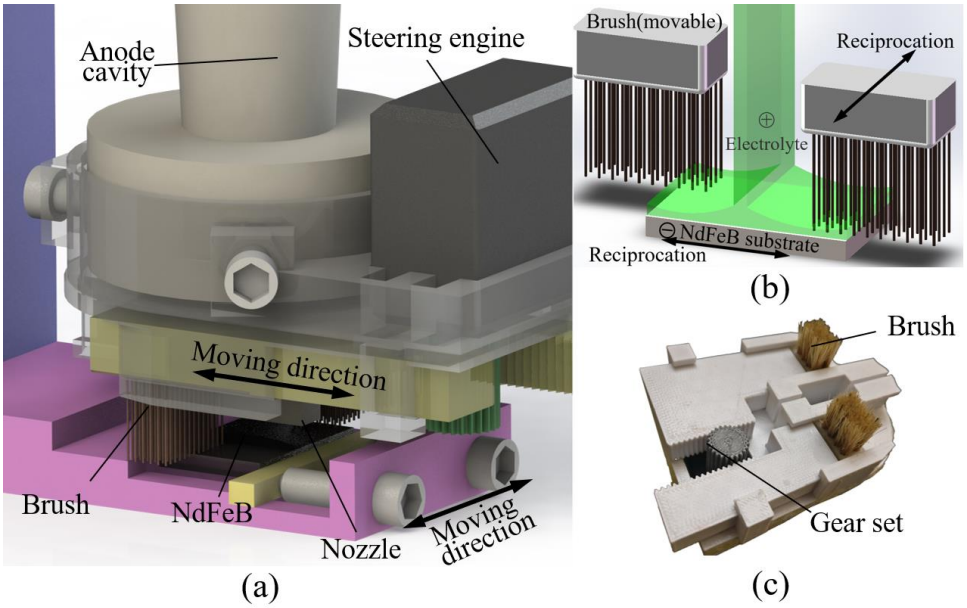

Figure 2. Friction device. (a) a diagram of a movable friction device, (b) a diagram of movable friction machining process, (c) a physical picture of a movable friction device.

The movable friction device is manufactured by 3D printing (Fig. 2c). The steering gear is used to drive the rack in order to achieve the reciprocating linear motion, which is perpendicular to the movement of the NdFeB, and provides online periodic the coating surface with friction during electrodeposition (Fig. 2a). The width of the brush is smaller than that of the nozzle to facilitate liquid

flow and prevent backflow between the two brushes. The double-sided movable friction also prevents from rubbing the surface of part of the workpiece in one-sided friction, which improves work efficiency. The experiment uses natural pig bristles to produce a flexible brush with a contact force of 2N, owing to its properties, including abrasion resistance, elasticity, and insulation[25, 26].

2.3 Experimental contents and parameters

In this experiment, a sintered NdFeB magnet measuring 20 mm×30 mm×3 mm is used. Prior to plating, the surface of the NdFeB magnet is polished with 400#-1200# silicon carbide sandpaper, dipped into an alkali degreasing solution to remove oil stain, ultrasonically cleaned with deionized water and alcohol, and infused into sealed molten zinc stearate for approximately half an hour. The material is ground with a ring polisher stepwise to a mirror finish, rinsed with deionized water and alcohol, and dried for subsequent use. The electrolyte consists of a dark nickel solution without additives. The composition is listed in Table 1, and the experimental parameters are listed in Table 2. To evaluate the effect of bilateral movable friction, non-friction, fixed friction, and movable friction—denoted by a, b, c, respectively—are compared.

Table 1. Plating solution composition.

Composition	Content(g/L)	Temperature (°C)	pH	Effect
$NiSO_4 \cdot 6H_2O$	280	50°C±1	4±0.1	Ni source
$NiCl_2 \cdot 6H_2O$	40			
H_3BO_3	40			pH buffer
NH_4OH				Adjust pH

Table 2. Processing parameters.

Parameters	Value
Nozzle size (mm)	20*1
Flow rate (L/h)	300
Machining gap (mm)	3
Scanning speed (mm/s)	12
Current (A)	0.2

2.4. Characterization of coatings

To evaluate the effect of different methods on the properties of the nickel plating, the coating properties are characterized using the test equipment listed in Table 3.

Table 3. Instruments and parameters.

Characterizations	Instruments	Parameters
Surface morphology	FESEM (S-4800)	5.0kV
Surface roughness	TR240	Number of times 3
Structure analysis	XRD (D/max 2500VL/PC)	20.0/80.0/0.02/0.12(sec) Cu(40 kV,100 mA)
Adhesion strength	Automatic scratch tester (WS-2005)	Load 40N
Corrosion resistance	Electrochemical workstation (CHI660E)	TAFEL&EIS

3. RESULTS ANALYSIS

3.1 Surface morphology

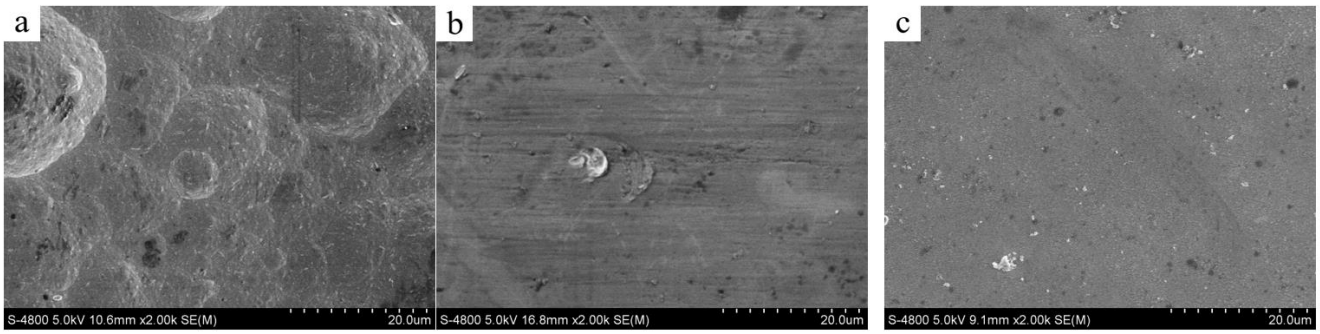

Figure 3. Coating surface morphology: (a) non-friction (b) fixed friction (c) movable friction

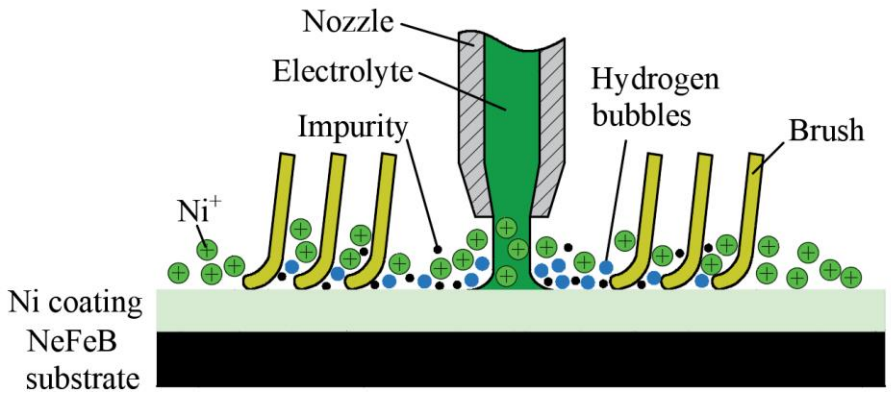

Figure 4. Schematic diagram of flexible friction.

In ordinary jet electrodeposition without friction assistance (Fig. 3a), the surface exhibits a considerable degree of roughness with numerous cellular bulges. The surface of the coating with

flexible friction (Figs. 3b, 3c) is relatively smooth, and has no apparent convex hull. This characteristic is attributed to the high current density of jet electrodeposition: when the nickel ions are deposited, hydrogen is generated together[13, 18]. These tiny hydrogen bubbles are adsorbed on the surface of the coating, affecting electrodeposition and eventually forming pinholes, pits, and other coating defects. Impurities in the solution can also come in contact with the coating surface and form nodules and pits on it. Once defects are formed, the protruding portion of the coating results in a larger curvature in the electric field lines, an increase in field strength, and the formation of a "edge effect"[15, 23]. Nickel ions become preferentially adsorbed and grow in the bumps, resulting in an uneven growth on the coating surface and surface defects.

Therefore, flexible friction assistance is introduced, as shown in Fig. 4. Under certain pressure conditions, the surface of the coating is rubbed to allow deposition with on-line friction to occur. The flexible brush generates relative motion with the workpiece under certain pressure, effectively removing the hydrogen and impurities generated by electrodeposition[27, 28]. The brushes are preferentially in contact with the protrusions of the coating, consequently exerting an electric field shielding effect on the protrusions. This occurrence reduces the charge that flows through the electrolyte from the nickel atoms and reduces the tip effect[25, 26]. Therefore, the surface of the flexible friction-assisted plating is flattened, no noticeable cellular bulges are present, and the surface is substantially improved. However, certain problems with the fixed friction device arise. As shown in Fig. 3b, the fixed brush and the workpiece only exhibit one-dimensional motion, and the brush repeatedly rubs the fixed trajectory, rendering the unidirectional brush marks conspicuous. To reduce brush marks on the plating surface, the friction device is eventually transformed into double-sided movable friction (Fig. 2). As the workpiece moves horizontally in the X direction, the brush is rubbed back and forth along the vertical direction and the direction of the movement of the workpiece. The surface of the workpiece can be rubbed randomly, which solves the problem of static friction easily generating fixed brush marks. As shown in Fig. 3c, the surface quality is the best. The surface roughness of the coating is closely related to the surface morphology.

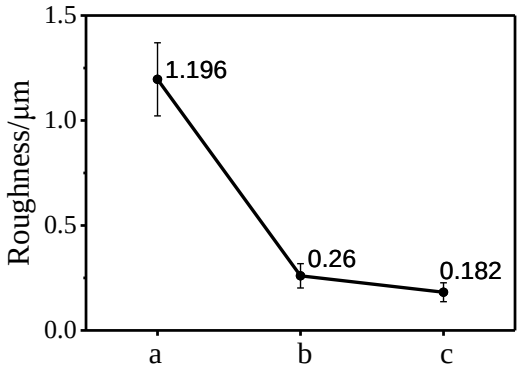

Figure 5. Surface roughness of the nickel coating

The roughness measurements of the coating surface are consistent with that of the microscopic surface (Fig. 5). In previous studies, the roughness of nickel coating is 0.7-3 μm[29, 30], and Biao Lv has reduced the roughness to 0.48 μm by flexible friction assisted electrodeposition[25]. In this study,

the frictionless device exhibits the highest roughness, reaching 1.196 μm. When fixed friction is added, roughness is reduced to 0.26 μm, and when movable friction is added, roughness is reduced to 0.182 μm.

3.2 Coating microstructure

The X-ray diffraction pattern of the nickel deposits is presented in Fig. 6. The preferred orientation of the deposits consists of the following texture coefficient TC(HKL).

$$TC_{hkl} = \frac{I_{(hkl)}/I_{0(hkl)}}{\sum_{i=1}^{n} I_{(hkl)}/I_{0(hkl)}} \times 100\% \quad (1)$$

where $I_{(hkl)}$ and $I_{0(hkl)}$ represent the X-ray diffraction intensities of the (hkl) planes of the nickel coatings and the standard nickel powder, respectively; n is the number of diffraction peaks. The greater the $TC_{(hkl)}$, the stronger the preferred orientation in the corresponding crystal plane of the nickel coating.

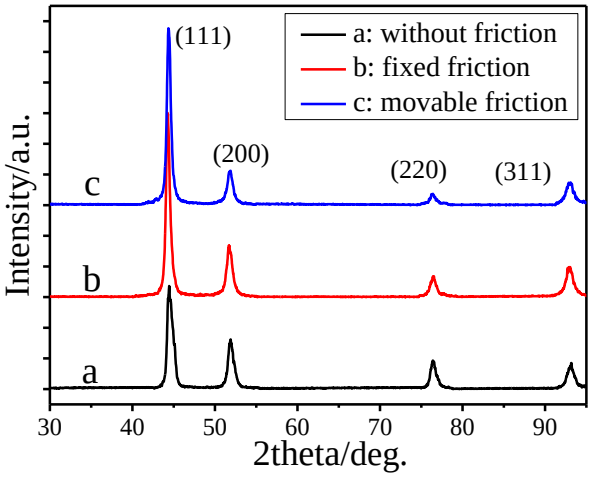

Figure 6. XRD patterns of the nickel coating

Table 4. Each crystal face texture coefficients of two kinds of nickel coating TC_{hkl}(%).

Nickel coating	(111)	(200)	(220)	(311)
Non-friction	22.1%	24.1%	28.9%	24.8%
Fixed friction	35.6%	22.0%	17.3%	25.1%
Movable friction	45.1%	19.2%	12.2%	23.4%

The calculation results (Table 4) indicate that compared with that of the Ni standard diagram, the preferential orientation of the (111) crystal plane of the dark nickel coating with frictional assistance is significantly stronger, the texture coefficient reaches 45.1%, and the (220) crystal plane is weakened. These findings show that flexible friction may change the crystal growth structure of the deposit and fully exert the growth ability of the (111) crystal plane. Biao Lv also concluded that the nickel coating electrodeposited with flexible friction has a (111) preferred orientation[26]. The (111)

crystal plane has a high atomic density and a low surface energy in the face-centered cubic structure, which is advantageous for improving the coating performance[16]. Furthermore, the decrease in current density leads to a significant increase in the preferred orientation of the (111) crystal plane[31, 32]. This occurrence is attributed to the addition of a friction brush, which allows the liquid to flow slowly and reflow around the nozzle. Nickel ions have more area on the surface of the workpiece to deposit at one time, relatively reducing the current density, improving the surface quality, and reducing various cellular bulges generated on the surface of the plating layer at a high current density.

3.3 Adhesion strength

To compare the effects of two types of friction on the bond strength of the coating, two workpieces are evaluated by plate adhesion testing to obtain the curve of the friction force against the applied load force (Fig. 7). When the diamond scribing needle scratches the coating and dissociates the coating from the substrate, the friction coefficient markedly changes. This behavior is reflected in the figure as a sudden change in the slope of the friction curve; that is, it can be used as the failure point of the film. As shown in Fig. 7, the static friction coating has a binding force of only 17.45 N, whereas the movable friction coating has a binding force of 26.75 N. It has been reported previously that Vitry prepared Ni coatings and the maximum binding force of the Ni coating was 21.8N[33]. Samples are cut using a wire-cutting machine, lightly ground and scrubbed with alcohol. The cross-sectional view is shown in Fig. 8. The fixed-friction coating has a distinct separation performance, and the movable friction coating remains closely attached to the NdFeB substrate; the combination is relatively good. Wei Jiang found that it was difficult to overcome the internal stress of nickel coating, so the coating adhesion strength was low and showed a clear gap between the pure Ni coating and NdFeB substrate[34]. This result is consistent with the conclusion on scratch testing. The reason is that the fixed-friction brush repeatedly rubs certain fixed locations and leaves brush marks on the surface (Fig. 3b). These fixed brush marks affect the compactness and adhesion strength. When the diamond stylus crosses these scratches, the surface of the coating becomes easier to scratch, resulting in reduced adhesion strength. Movable friction avoids fixed brush marks on the surface coating. The frictional position of the coating exhibits randomness, rendering the coating more uniform and consequently enhancing the adhesion strength of the coating.

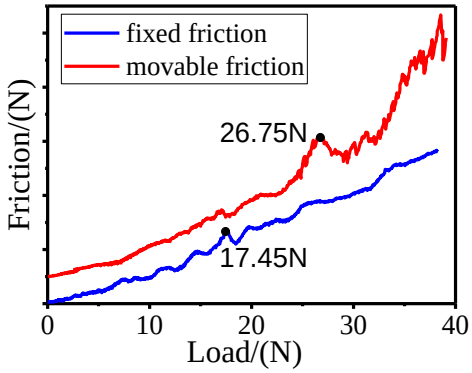

Figure 7. Adhesion strength test curves measured by scratch tester

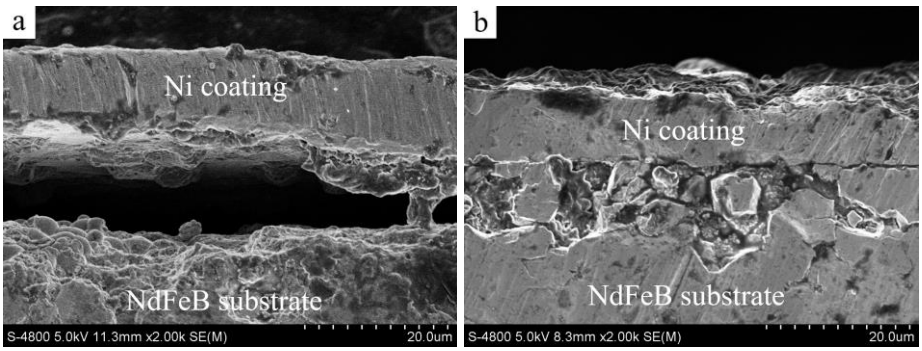

Figure 8. Ni coating on Sintered NdFeB (a) fixed friction (b) movable friction

3.4 Corrosion behavior

Potentiodynamic polarization curves of different coatings in a 3.5 wt% NaCl solution are presented in Fig. 8(a). The corrosion potential (E_{corr}) and the corrosion current (i_{corr}) are derived from the intersection of the tangents of the cathode and anode Tafel curves shown in Table 5. Without frictional aid, the E_{corr} of the coating has the most negative value, whereas i_{corr} has the largest value. The corrosion resistance with flexible friction improves, and the corrosion current density decreases from 104.5 $\mu A \cdot cm^{-2}$ to 28.75 $\mu A \cdot cm^{-2}$. Jun Zhu analyzed the coating microstructure and the results showed that nickel prepared by friction assisted jet electrodeposition had a compact structure and a better electrochemical corrosion resistance [35, 36]. From a kinetic point of view, the precondition for the protective coating of the cathodic coating must be non-porous to provide mechanical isolation protection. However, owing to hydrogen evolution from the cathode, impurities, and tip effect during jet electrodeposition, cracks, voids, or columnar gaps are found in the nickel coating (Fig. 3a), and Cl^- can easily follow these plating defects or weaknesses, which could quickly erode to the surface of the substrate, accelerating the corrosion of the substrate, thereby increasing the corrosion current density.

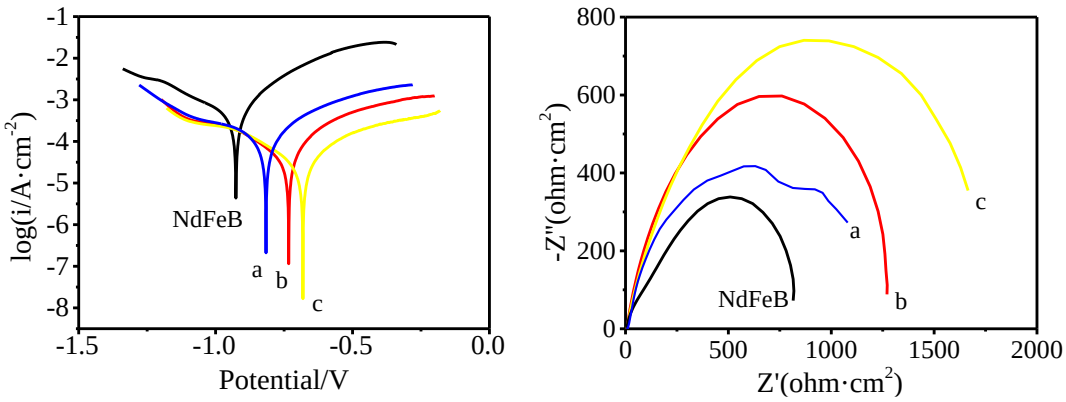

(a) (b)

Figure 9. (a)Polarization curves(scan rate: 1mV/s) and (b)Nyquist plots(frequency range: 10^5-10^{-2} Hz) of the nickel coating on NdFeB in 3.5 wt% NaCl solution.a: non-friction, b: fixed friction, c: movable friction.

The coating produced using friction-assisted jet electrodeposition has few surface defects, and the corrosive medium hardly enters the substrate, preventing the solution from attacking the NdFeB substrate, thereby improving the corrosion resistance of the coating. Electrochemical impedance spectra in a 3.5 wt% NaCl solution are examined and are shown as the impedance curve in Fig. 9(b). The radius of the capacitive loop with a flexible friction coating is larger than that of the capacitive loop with no friction, and the surface has a flexible friction assisted with higher polarization resistance; that is, higher corrosion resistance. This change is consistent with the changes in the Tafel curve.

Table 5. Corrosion potential and corrosion current density

Samples	E_{corr}/V	i_{corr}/μA/cm^2
NdFeB	-0.926	497.0
a: Non-friction	-0.816	104.5
b: Fixed friction	-0.733	48.05
c: Movable friction	-0.681	28.75

To better reflect the anti-corrosion performance, the sample is placed in a 3.5 wt% NaCl solution and allowed to stand for 48 h. The surface after etching is shown in Fig. 10. The frictionless auxiliary spray electrodeposition has micropores and microcracks on the surface itself, which leads to rapid corrosion of the surface material, hence the numerous corrosion pits on the surface. Wei Zhuo found the corrosive solution penetrate the coating surface through nodules easily which lead to a rapid corrosion [27]. Fixed friction helps because of the presence of fixed scratches. Once corrosion occurs, it is “diffused” along the direction of the scratch, which also seriously affects the corrosion resistance of the coating. The movable friction-assisted coating surface has occasional corrosion pits that are considerably smallest, and the rest of the surface remains intact. Thus, compared with conventional jet electrodeposition, on-line flexible, movable friction can largely reduce the number of surface defects. In addition, the coating becomes smoother and more compact, impeding corrosion attack. Despite the presence of corroded areas, other parts cannot be easily affected, which greatly improves the corrosion resistance of the nickel coating.

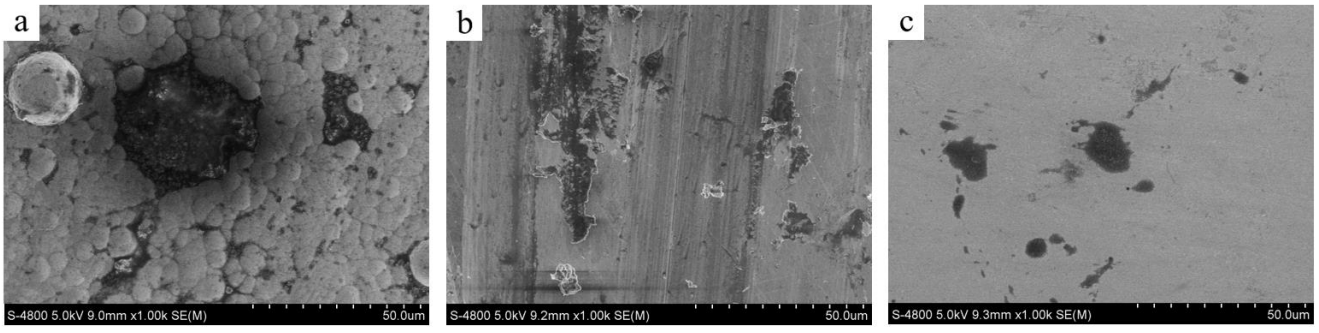

Figure 10. Coating with the immersion time of 48 h in 3.5 wt% NaCl solution. a: non-friction, b: fixed friction, c: movable friction.

4. CONCLUSIONS

1) Compared with conventional jet electrodeposition, flexible friction-assisted jet electrodeposition can effectively reduce the formation of defects and improve the surface quality of the coating. The surface tends to be flat, and the roughness is markedly reduced, significantly improving the surface quality.

2) Flexible friction-assisted jet electrodeposition influences the growth structure of the coating grain. Compared with traditional jet electrodeposition, it clearly exhibits (111) preferred orientation, and its texture coefficient is as high as 45.1%.

3) Compared with static friction, movable friction provides the coating with adhesion strength increased from 17.45 N to 26.75 N.

4) The coatings produced by flexible friction-assisted jet electrodeposition exhibit higher corrosion resistance. Compared with the fixed flexible friction method, the proposed double-side flexible movable friction method results in a more uniform friction, higher efficiency, and higher corrosion resistance. In addition, the corrosion current decreases to 28.75 $\mu A/cm^2$.

ACKNOWLEDGEMENTS
This work was supported by the National Natural Science Foundation of China (No. 51475235, No. 51105204 and No. U1537105) and the Key Research and Development Plan of Jiangsu Province (BE2016010-3).

References

1. M. Sagawa, S. Fujimura, N. Togawa, H. Yamamoto, *J. Appl. Phys.*, 55 (1984) 2083.
2. C. Ren, W. Jin, H. Zhou, J. Li, X. Song, *Chinese J. Rare Meta.*, 32 (2013) 249.
3. T. Zhang, F. Chen, Y. Zheng, H. Wen, J. Wang, L. Zhang, L. Zhou, *Intermetallics*, 73 (2016) 67.
4. B. Ma, A. Sun, Z. Lu, C. Cheng, C. Xu, *J. Magn. Magn. Mate.*, 416 (2016) 150.
5. S. Zhang, Y. Zou, *Mate. Prot*., 32 (1999) 28.
6. Y.W. Song, H. Zhang, H.X. Yang, Z.L. Song, *Mate. Corros*., 59 (2015) 794.
7. W. Fernengel, W. Rodewald, R. Blank, P. Schrey, M. Katter, B. Wall, *J. Magn. Magn. Mate.*, 196 (1999) 288.
8. L.Q. Yu, Y.H. Wen, M. Yan, *J. Magn. Magn. Mate.*, 283 (2004) 353.
9. A. Ali, A. Ahmad, K.M. Deen, *Mate. Corros*., 61 (2015) 130.
10. L. Song, Y. Wang, W. Lin, Q. Liu, *Surf. Coat. Tech.*, 202 (2008) 5146.
11. Z. Chen, A. Ng, J. Yi, X. Chen, *J. Magn. Magn. Mate.*, 302 (2006) 216.
12. C.L. Ban, X. Shao, J. Ma, H. Chen, *T. Nonferr. Metal. Soc*., 22 (2012) 1989.
13. G.F. Wang, L.D. Shen, Y.H. Huang, *Int. J. Electrochem. Sc*., 7 (2012) 10818.
14. H. Gvl, M. Uysal, H. Akbulut, A. Alp, *Surf. Coat. Tech.*, 258 (2014) 1202.
15. X. Liu, L. Shen, M. Qiu, Z. Tian, Y. Wang, K. Zhao, *Surf. Coat. Tech.*, 305 (2016) 231.
16. L. Shen, K. Zhao, M. Qiu, X. Wang, M. Fan, *Int. J. Electrochem. Sc*., 13 (2018) 984.
17. L. Shen, C. Wang, Z. Tian, W. Jiang, W. Zhuo, K. Zhao, *Int. J. Electrochem. Sc*., 13 (2018) 1831.
18. X. Zheng, M. Wang, H. Song, D. Wu, X. Liu, J. Tan, *Surf. Coat. Tech.*, 325 (2017) 181.
19. I. Tudela, Y. Zhang, M. Pal, I. Kerr, A.J. Cobley, *Surf. Coat. Tech.*, 259 (2014) 363.
20. I. Tudela, Y. Zhang, M. Pal, I. Kerr, T.J. Mason, A.J. Cobley, *Surf. Coat. Tech.*, 264 (2015) 49.
21. B. Bakhit, A. Akbari, F. Nasirpouri, M.G. Hosseini, *Appl. Surf. Sci*., 307 (2014) 351.
22. Y. Wang, L. Shen, M. Qiu, Z. Tian, X. Liu, W. Zhuo, *J. Electrochem. Soc.*, 163 (2016) D579.

23. K. Zhao, L. Shen, M. Qiu, Z. Tian, W. Jiang, *Int. J. Electrochem. Sc.*, 12 (2017) 8578.
24. J. Zhu, Z.J. Tian, Z.D. Liu, L.D. Shen, Y.H. Huang, G.F. Wang, *J. South China U. Tech.*, 39 (2011) 92.
25. B. Lv, Z. Hu, X. Wang, B. Xu, *Surf. Coat. Tech.*, 270 (2015) 123.
26. B. Lv, Z. Hu, X. Wang, B. Xu, *T. Nonferr. Metal. Soc.*, 25 (2015) 3297.
27. W. Zhuo, L. Shen, M. Qiu, Z. Tian, W. Jiang, *Surf. Coat. Tech.*, 333 (2018) 87.
28. Y. Deng, L. Biao, X.H. Wang, H.U. Zhen-Feng, X.B. Liang, *Electroplating. Finish.*, 19 (2016) 1021.
29. P. Narasimman, M. Pushpavanam, V.M. Periasamy, *Wear*, 293 (2012) 197.
30. N.P. Wasekar, P. Haridoss, S.K. Seshadri, G. Sundararajan, *Surf. Coat. Tech.*, 291 (2016) 130.
31. Y. Pan, J. Shan, C. Dai, *T. Nonferr. Metal. Soc.*, 17 (2007) 770.
32. N.A. Pangarov, *J. Electrochem. Soc.*, 9 (1965) 70.
33. V. Vitry, F. Delaunois, C. Dumortier, *Surf. Coat. Tech.*, 202 (2008) 3316.
34. W. Jiang, L.Shen, M. Qiu, X.Wang, M. Fan, Z. Tian, *J. Alloy. Compd.*, 762 (2018) 115.
35. J. Zhu, L. Shen, Z. Tian, Z. Liu, Y. Huang, G. Wang, *Rare. Metal. Mat. Eng.*, 42 (2013) 2371.
36. L. Shuai, P. Mathé, *Chinese J. Nonferr. Metal.*, 23 (2013) 1618.